TITLE:

Discovery of primitive CO2-bearing fluid in an aqueously altered carbonaceous chondrite

AUTHOR(S):

Tsuchiyama, Akira; Miyake, Akira; Okuzumi, Satoshi; Kitayama, Akira; Kawano, Jun; Uesugi, Kentaro; Takeuchi, Akihisa; Nakano, Tsukasa; Zolensky, Michael

CITATION:

Tsuchiyama, Akira ...[et al]. Discovery of primitive CO2-bearing fluid in an aqueously altered carbonaceous chondrite. Science Advances 2021, 7(17): eabg9707.

ISSUE DATE:

2021-04

URL:

http://hdl.handle.net/2433/262728

RIGHT:

Copyright © 2021 The Authors, some rights reserved; exclusive licensee American Association for the Advancement of Science. No claim to original U.S. Government Works.; Distributed under a Creative Commons Attribution NonCommercial License 4.0.

京都大学学術情報リポジトリ
KURENAI 紅
Kyoto University Research Information Repository

京都大学 KYOTO UNIVERSITY
A Self-archived copy in
Kyoto University Research Information Repository
https://repository.kulib.kyoto-u.ac.jp
京都大学学術情報リポジトリ KURENAI 紅 Kyoto University Research Information Repository

SCIENCE ADVANCES | RESEARCH ARTICLE

SPACE SCIENCES

Discovery of primitive CO_2-bearing fluid in an aqueously altered carbonaceous chondrite

Akira Tsuchiyama[1,2,3]*, Akira Miyake[4], Satoshi Okuzumi[5], Akira Kitayama[4], Jun Kawano[6], Kentaro Uesugi[7], Akihisa Takeuchi[7], Tsukasa Nakano[8], Michael Zolensky[9]

Copyright © 2021 The Authors, some rights reserved; exclusive licensee American Association for the Advancement of Science. No claim to original U.S. Government Works. Distributed under a Creative Commons Attribution NonCommercial License 4.0 (CC BY-NC).

Water is abundant as solid ice in the solar system and plays important roles in its evolution. Water is preserved in carbonaceous chondrites as hydroxyl and/or H_2O molecules in hydrous minerals, but has not been found as liquid. To uncover such liquid, we performed synchrotron-based x-ray computed nanotomography and transmission electron microscopy with a cryo-stage of the aqueously altered carbonaceous chondrite Sutter's Mill. We discovered CO_2-bearing fluid (CO_2/H_2O > ~0.15) in a nanosized inclusion incorporated into a calcite crystal, appearing as CO_2 ice and/or CO_2 hydrate at 173 K. This is direct evidence of dynamic evolution of the solar system, requiring the Sutter's Mill's parent body to have formed outside the CO_2 snow line and later transportation to the inner solar system because of Jupiter's orbital instability.

INTRODUCTION

Water is abundant as solid ice in the solar system, providing evidence that water exists in the solar system, consistent with observed aqueous alteration in primitive meteorites and formation of the Earth's ocean, and liquid water closely relates to the origin of life. Not only H_2O ice but also CO_2 and CO ice define the particular distances from the Sun in the early solar system called snow lines (SLs) beyond which it was cold enough for these volatile components to condense into ice grains. If we know the composition of such ice (e.g., CO_2/H_2O ratio) recorded in primitive meteorites, we can distinguish between formation inside or outside of the SL (*1*).

Most meteorites originate from asteroids that formed as planetesimals in the early solar system (*2*). Minerals and ice were accreted together outside the SL to form planetesimals. Aqueous alteration by reaction of melted ice with anhydrous minerals occurred and was recorded in some primitive meteorites called carbonaceous chondrites (CCs) [e.g., (*3*)]. Water is mostly present as hydroxyl and/or H_2O molecules of hydrous minerals. It is expected that liquid water should remain as fluid inclusions in minerals (e.g., calcite: $CaCO_3$) that precipitated in aqueous fluid. However, completely verified fluid inclusions in CCs have not been recognized so far (*4*). The only fluid inclusions from the early solar system were found in halite (NaCl) associated with CC clasts in less primitive ordinary chondrites (*5*, *6*). Here, we report the presence of CO_2-bearing fluid inclusion in a calcite grain of an aqueously altered CC [the Sutter's Mill meteorite; Mighei-type (CM) chondrite] and use the results to infer the origin of the meteorite parent body.

[1]Research Organization of Science and Technology, Ritsumeikan University, 1-1-1 Nojihigashi, Kusatsu, Shiga 525-8577, Japan. [2]CAS Key Laboratory of Mineralogy and Metallogeny/Guangdong Provincial Key Laboratory of Mineral Physics and Materials, Guangzhou Institute of Geochemistry, Chinese Academy of Sciences, 511 Kehua Street, Wushan, Tianhe District, Guangzhou 510640, China. [3]CAS Center for Excellence in Deep Earth Science, 511 Kehua Street, Wushan, Tianhe District, Guangzhou, 510640, China. [4]Department of Earth and Planetary Sciences, Graduate School of Science, Kyoto University, Kitashirakawa-Oiwakecho, Sakyo-ku, Kyoto 606-8502, Japan. [5]Department of Earth and Planetary Sciences, School of Science, Tokyo Institute of Technology, 2-12-1 Ookayama, Meguro-ku, Tokyo 152-8551, Japan. [6]Department of Earth and Planetary Sciences, Faculty of Science, Hokkaido University, Kita-10 Nishi-8, Kita-ku, Sapporo 060-0810, Japan. [7]Japan Synchrotron Radiation Research Institute, Hyogo 679-5198, Japan. [8]Geological Survey of Japan, National Institute of Advanced Industrial Science and Technology, Ibaraki 305-8567, Japan. [9]Astromaterials Research and Exploration Science, NASA Johnson Space Center, Houston, TX 77058, USA.
*Corresponding author. Email: atsuchi@fc.ritsumei.ac.jp, atsuchi@gig.ac.cn

RESULTS

Micrometer- and nanosized inclusions in calcite grains

We conducted a specific analysis protocol (fig. S1) to search for fluid inclusions, systematically combining scanning electron microscopy (SEM), focused-ion beam (FIB) microsampling, synchrotron radiation–based x-ray computed nanotomography (SR-XCT), scanning transmission electron microscopy with energy-dispersive spectroscopy (STEM/EDS), and TEM with cryo-stage (cryo-TEM).

We examined polished sections of Sutter's Mill and searched for calcite (Fig. 1A and fig. S1) appropriate for the present analysis. Seven grains ~30 to 50 μm in size were selected and extracted using FIB to make equant samples with side length of ~30 μm (Fig. 1B and fig. S1). The samples were imaged using SR-XCT to obtain their three-dimensional (3D) images with absorption and phase-shift contrasts using two different methods: dual-energy tomography (DET) (*7*) and scanning-imaging x-ray microtomography (SIXM) (*8*) with ~70 and 100 nm in voxel size, respectively (*3*). A large number of inclusions in the interior of calcite grains were recognized in 3D (Fig. 1, B and C). They are divided into two types: micrometer- and nanosized inclusions typically about or more than a few micrometers and about or less than a few hundred nanometers in size, respectively. Micrometer-sized inclusions are usually irregular (Fig. 1E) or subspherical (Fig. 1F) in shape and more or less have facets. Some are hexagonal platelets (negative crystals) with basal faces of probably {001} (Fig. 1G). The values of refractive index decrement (RID) in phase-shift images are closely proportional to material density (RID = 8.88×10^{-6}, 3.62×10^{-6}, 2.51×10^{-6}, and 4.2×10^{-9} at 8 keV for calcite, water, liquid CO_2, and air, respectively). The RID values of micrometer-sized inclusions are less than that of water and liquid CO_2, indicating no trapped fluid inside (m-inc in A-A′: Fig. 1D).

Nanosized inclusions are located in specific regions (Fig. 1, B and C), and they are too small to confirm the presence of fluid by SR-XCT. We extracted ultrathin sections of nanosized inclusion-rich regions of two XCT samples using FIB and observed them by TEM. We also extracted TEM sections from five calcite grains without performing SR-XCT (fig. S1). The typical inclusion sizes range

Downloaded from http://advances.sciencemag.org/ on May 6, 2021

京都大学 KYOTO UNIVERSITY
A Self-archived copy in
Kyoto University Research Information Repository
https://repository.kulib.kyoto-u.ac.jp
京都大学学術情報リポジトリ KURENAI 紅 Kyoto University Research Information Repository

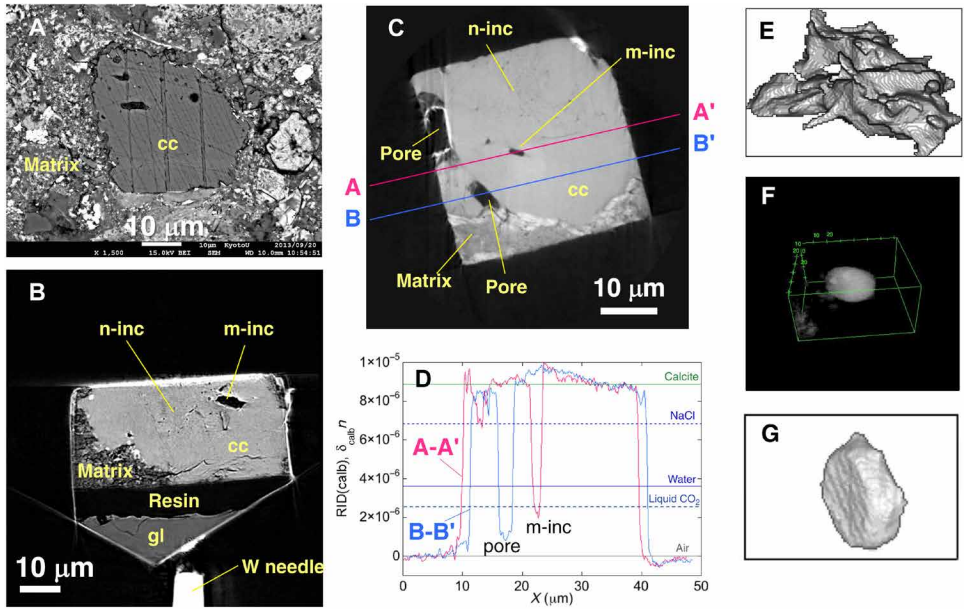

Fig. 1. SEM and XCT slice images of calcite grains, line profiles of RID values, and bird's-eye views of micrometer-sized inclusions. (**A**) A backscattered electron SEM image shows a typical calcite grain (CC-7; see Materials and Methods for the sample number) in matrix. Micrometer-sized inclusions and a large number of nanosized inclusions are observed in an absorption XCT image at 7 keV of CC-7 (**B**) and a phase-shift image of CC-25 (**C**). (**D**) Line profiles of RID values along A-A′ and B-B′ in (C). The RID values larger than zero are due to size effects (see Materials and Methods). Bird's-eye views of micrometer-sized inclusions obtained from XCT images have a variety of morphologies, from irregular [(**E**): CC-7], subspherical with facets [(**F**): CC-27], and tabular hexagonal (negative crystal) [(**G**): m-inc in (C)]. cc, calcite; m-inc, micrometer-sized inclusion; n-inc, nanosized inclusions; gl, slide glass.

from <10 to a few hundred nanometers (Fig. 2). The thickness of the section is ~300 nm to prevent the inclusions from decrepitating (bursting). Some inclusions are distributed as band-like growth zoning or healed fractures (Fig. 2A), and some are located along twin boundaries (Fig. 2B). Most of them have ovoidal shapes with facets (Fig. 2D) probably of calcite {001} plane (fig. S2). Some inclusions contain trapped or daughter crystals (Fig. 2D), which seem to be Na-Mn and Fe sulfates, FeOOH (or Fe_2O_3) (fig. S3), and apatite (fig. S4) based on their EDS spectra.

Discovery of CO_2-bearing fluid inclusion

Then, we made TEM observations using a cryo-TEM on relatively large inclusions that may preserve fluid, <100 nm in size, apart from twin boundaries, and having relatively dark contrast in TEM bright-field images. In one inclusion (arrow in Fig. 2C), we found three selected-area electron diffraction (SAED) spots at 173 K that were not observed at 293 K (yellow and red arrows in Fig. 3A). When heated to 293 K, the three spots disappeared (Fig. 3B). After keeping the sample at room temperature for 33 days, we found two new spots (red arrows in Fig. 3C). After cooling to 173 K again, the two spots disappeared and three new spots appeared (dashed red and yellow arrows, respectively, in Fig. 3D). When heated to 293 K again, the three spots disappeared (Fig. 3E). The extra spots appearing at 173 K cannot be indexed by H_2O ice (cubic and hexagonal) or $CaCO_3$ polymorphs (calcite, aragonite, etc.) but are successfully indexed as CO_2 [$0\bar{1}1$] ice or CO_2 hydrate (CO_2·5.75H_2O) indicating freezing of H_2O-CO_2 fluid. This is consistent with the CO_2 melting point (~218 K) or the CO_2 ice–CO_2 hydrate eutectic point (~216 K) (*9*). The possibility of CH_4 and CO ice can be excluded because of their low

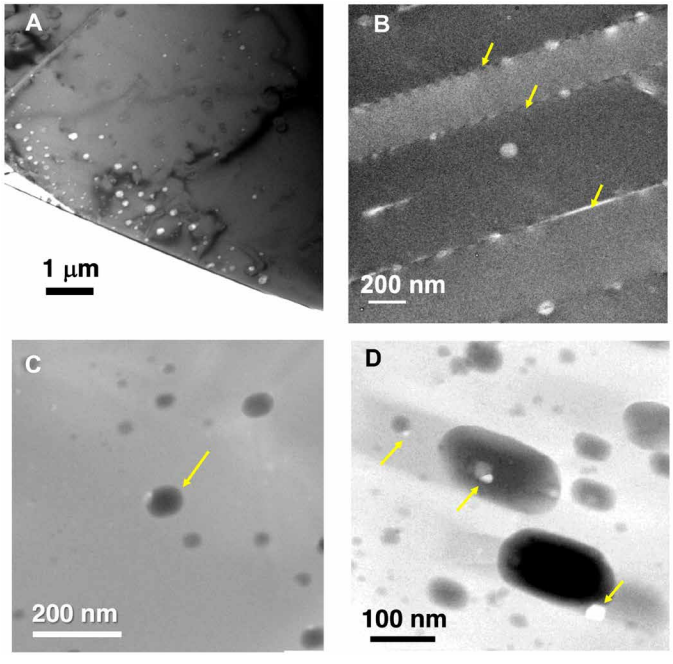

Fig. 2. TEM images of nanosized inclusions in calcite. Some nanosized inclusions are distributed as bands [(**A**): bright-field (BF) image of CC-15] and along twin boundaries [(**B**): arrows, BF image of calcite CC-6]. One inclusion [(**C**): arrow, STEM image of C7K] has extra diffraction spots in cryo-TEM observation (Fig. 3). Nanosized inclusions have ovoidal shapes with facets [(**D**): STEM image of CC-7]. Tiny faceted objects as trapped or daughter crystals are observed [(C) and arrows in (D); see also fig. S3].

Downloaded from http://advances.sciencemag.org/ on May 6, 2021

京都大学 KYOTO UNIVERSITY
A Self-archived copy in
Kyoto University Research Information Repository
https://repository.kulib.kyoto-u.ac.jp
京都大学学術情報リポジトリ KURENAI 紅 Kyoto University Research Information Repository

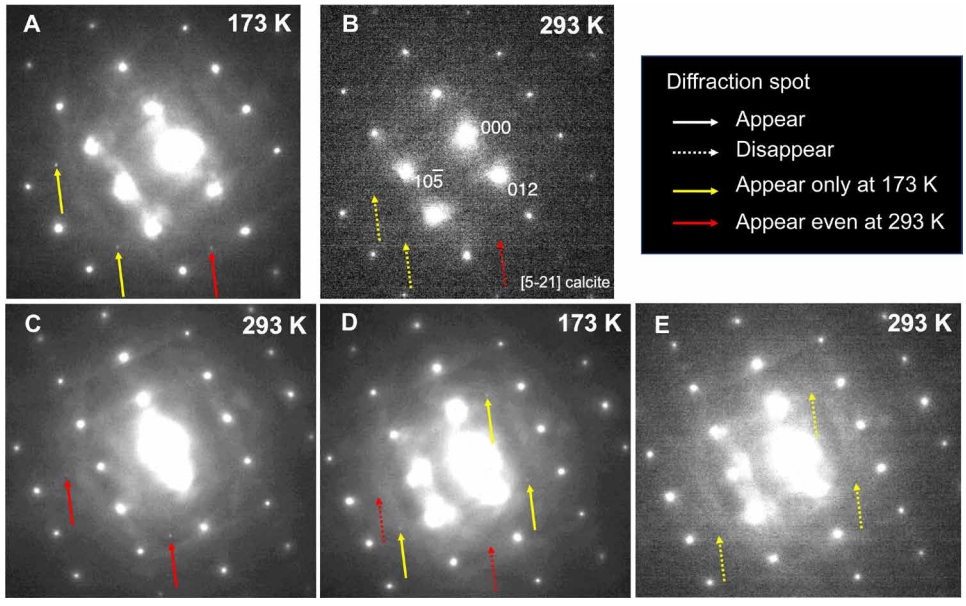

Fig. 3. Change in SAED patterns of a nanosized inclusion in cryo-TEM. SAED patterns of an area including a nanosized inclusion in Fig. 2C (arrow) cooled at 173 K (**A**), raised to 293 K (**B**), kept for 33 days at 293 K (**C**), cooled again at 173 K (**D**), and raised to 293 K (**E**) are shown. Yellow and red arrows show that spots appeared only at 173 K and after keeping the sample at 293 K, respectively.

melting points, 90.5 K (*10*) and 70 K (*11*), respectively. The peaks appearing at 293 K can be explained by a metastable $CaCO_3$ phase (aragonite $[\bar{4}\,\bar{2}3]$ or vaterite) or monohydrocalcite ($CaCO_3{\cdot}H_2O$). This phenomenon can be explained by dissolution and reprecipitation of a $CaCO_3$ phase with nucleation delay during cooling and heating, respectively, and the negative temperature dependence of $CaCO_3$ phase solubilities (*12*) (see "Process occurring in the cryo-TEM observation" in Supplementary Text, fig. S5, and table S1). No elements other than those detected in the host calcite were detected in this inclusion by STEM/EDS except for a very small amount of P. We observed a tiny grain, probably of trapped apatite, in this P-bearing region (Fig. 2C). However, no diffraction spots corresponding to this grain were recognized because we did not observe any steady spots at 297 and 173 K.

DISCUSSION

Origin of CO_2-bearing fluid

Micrometer- and nanoinclusions with facets (Figs. 1, F and G, and 2) strongly suggest the presence of original fluid; facets formed from irregular interface (Fig. 1E) by dissolution and precipitation of calcite in fluid make the interfacial energy smaller, and finally, negative crystals (Fig. 1G) are formed. The calcite-water interface with the minimum energy is {104} based on atomistic simulations (*13*) and is different from {001} observed in the present inclusions (fig. S2). This could be due to the CO_2-bearing fluid, which may change the interfacial energies. Sulfate grains (fig. S3) might precipitate in such a fluid. Fluid easily escaped from inclusions along cleavages and/or twin boundaries by mechanical disturbances during the long history of the meteorite (~4.5 billion years). Large faceted pores along calcite-matrix boundaries (P in B-B′; Fig. 1D) might also have originally been fluid-filled. Nanosized inclusions have a good chance to preserve fluids because of their small size and large numbers, although the probability is not large because we found fluid only in one inclusion among the seven examined samples.

The origin of CO_2 in the CO_2-bearing fluid is probably (1) oxidation of organics and (2) CO_2 ice (*1*). The former contribution should be very small because strong oxidants are required and the maximum amount of CO_2 is expected to be only ~0.1 weight % (wt %) in CCs (*1*). In addition, the degree of thermal metamorphism of the present sample is so low that the formation of a sufficient amount of CO_2 is not expected from organics. In contrast, CO_2 ice was abundant in the early solar system and is one of the major C-bearing molecules in comets (CO_2/H_2O ~0.03 to 0.3) (*14*).

The observed CO_2 ice and/or CO_2 hydrate assemblage is reasonable at temperatures <~218 K with the molecular CO_2/H_2O ratio >~0.15 based on the phase diagram of CO_2-H_2O (*9*), indicating that the CO_2/H_2O ratio of the fluid is ~0.15 or larger. Selective escape of H_2O and enrichment of CO_2 in fluid inclusions in terrestrial quartz have been reported (*15*). However, this possibility can be eliminated because we did not observe any void in the inclusion (Fig. 2C). The mean CO_2/H_2O ratio of ice originally present in CCs was estimated to be 0.012 for 45 CM chondrites (Sutter's Mill not included) from the $^{13}C/^{12}C$ ratio of carbonates (calcite and dolomite) (*1*). However, this ratio is dependent on the assumption of the isotope ratios of CO_2 ice and an unknown C-source. The large CO_2/H_2O ratio (>~0.15) is appropriate at least for Sutter's Mill ice because the ratio is based on the phase diagram (*9*).

CO_2-bearing fluid was plausibly present during aqueous alteration in the interior of an asteroid. According to the phase diagram (*9*), at aqueous alteration temperatures of CMs [~270 to 300 K (*16*)], CO_2-bearing water (W: ~5 mol % CO_2) coexists with nearly pure CO_2 liquid (L) or fluid (F: as a liquid-gas mixture) at pressures >~50 bars or >~200 bars, which correspond to asteroids >~100 km and >~200 km in diameter, respectively (see "Conditions for aqueous alteration and the characteristics of "fluid" in the nano-inclusion" in Supplementary Text and table S2). Calcite could precipitate from

Downloaded from http://advances.sciencemag.org/ on May 6, 2021

京都大学 KYOTO UNIVERSITY
A Self-archived copy in
Kyoto University Research Information Repository
https://repository.kulib.kyoto-u.ac.jp
京都大学学術情報リポジトリ KURENAI 紅 Kyoto University Research Information Repository

W or F, but the incorporation of W or F alone cannot explain the CO_2/H_2O ratio of the nanoinclusion or the carbonate appearance by heating (Fig. 3), respectively. Accordingly, a W + L or W + F mixture should be incorporated during calcite precipitation. Because F is very mobile, W + F mixture is favorable, suggesting a parent body >~200 km in diameter.

Formation of SMPB beyond the CO_2 SL and its astronomical significance

CO_2-rich ice in Sutter's Mill indicates that its parent body formed outside the CO_2 SL in the early solar system. We may exclude the possibility of direct origin from a comet (or mixture of comet and silicate body) because we do not have any evidence of CO, which is another major C-bearing molecule in comets (*14*). The H_2O, CO_2, and CO SLs are roughly determined by the condensation temperatures (~160, ~75, and ~22 K, respectively) (*17*). Assuming that the temperature of the solar nebula was determined by internal viscous heating in addition to solar irradiation (see "Calculation of H_2O, CO_2 and CO snow lines" in Supplementary Text), their locations moved toward the Sun as the nebula accretion rate $\dot{M}$ decreased with time (Fig. 4). H_2O (and CO_2) ice should be absent for $\dot{M} < \sim 5 \times 10^{-9}$ mass of the Sun ($M_\odot$)/year because Earth does not have abundant H_2O (and CO_2). Thus, Sutter's Mill's parent body (SMPB) should have formed at >3 to 4 astronomical units (au) from the Sun but at <~50 au as CO is not in the fluid (Fig. 4).

Recent dynamic models of solar system evolution have proposed that volatile-rich asteroids formed in the outer solar system beyond Jupiter's orbit and were subsequently transported into the inner region, where the asteroids are currently located in the main asteroid belt, because of an orbital instability of the giant planets (*18*, *19*). A dichotomy in isotopic compositions of rock-forming elements between CCs and non-CCs also suggested formation regions outside and inside of Jupiter, respectively (*20*, *21*). The present result gives direct evidence of such a dynamic model. However, this does not necessarily imply that SMPB formed at >~10 au like a trans-Neptunian object (*21*). If SMPB formed beyond Jupiter's core that formed earlier, SMPB could collect CO_2 ice. It should be noted that CO_2 (and H_2O) ice could not migrate inward across Jupiter's core. Assumption of Jupiter's core formation in the early stage at ~3 au is based on the distribution of refractory elements and inclusions in meteorites, which requires that CM parent bodies formed at 3.76 au within CO_2 SL (*22*).

Carbonates are commonly present in some CCs—CM, Ivuna-type (CI), and the Tagish Lake meteorite (C ungrouped)—but are rare in Renazzo-type (CR) and Vigarano-type (CV) or absent in Ornans-type (CO) and the Acfer 094 meteorite (C ungrouped) (*16*). If carbonates precipitated from CO_2-bearing fluid originating from CO_2-bearing ice, CI and Tagish Lake might have also formed outside the CO_2 SL. The CO_2/H_2O ratio of Tagish Lake ice estimated from the carbon isotopic ratio is large (~0.24) (*1*).

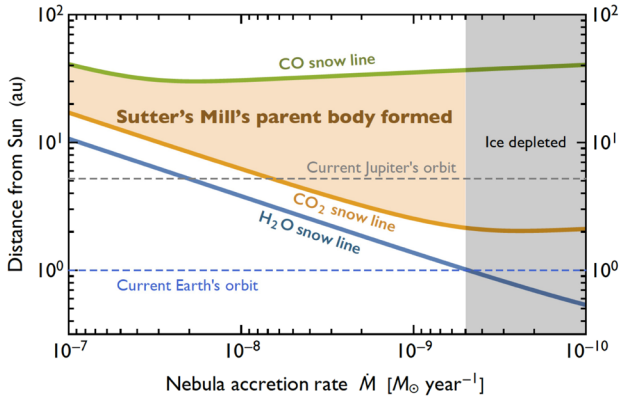

Fig. 4. H_2O, CO_2, and CO SLs and SMPB formation. During the evolution of the early solar system, nebular accretion rate, $\dot{M}$, decreased with time and the distances of the SLs from the Sun decreased. A possible region of SMPB formation is bounded by CO_2 and CO SLs and the ice-depleted region.

MATERIALS AND METHODS

Samples

Two polished thin sections of a CM2 clast of Sutter's Mill (CM2) were used in this study. One is small (~1 mm by ~1 mm) and the other [SM51 in (*23*)] is large (~18 mm by ~22 mm). This particular sample was collected immediately after the fall, and terrestrial formation of carbonates is precluded.

Experimental design

To search for inclusions in calcite grains of the Sutter's Mill meteorite and obtain their mineralogical characteristics, we performed systematic analyses combining field-emission SEM (FE-SEM), FIB microsampling, SR-XCT, and field-emission (scanning) TEM (FE-S/TEM) using a stage at room temperature (S/TEM) and a cryo-stage (cryo-S/TEM) (fig. S1). This method was originally developed by Miyake *et al.* (*24*). We adopted two types of analytical flow: one is (1) FE-SEM, (2) FIB microsampling, (3) SR-XCT, (4) FIB thinning, and (5) S/TEM and cryo-S/TEM and the other is one that skips processes (2) and (3). The former is essentially similar as described in (*3*). The details for each analysis are as follows.

FE-SEM observation

We observed the polished sections using an FE-SEM (JEOL, JSM-7001F, at Kyoto University) equipped with energy-dispersive x-ray spectroscopy (EDX) (Oxford Instruments, X-Max^N 150 mm^2) operated at 10 kV and selected 12 calcite grains belonging to type 1 (*25*) ~30 to 50 μm in size (CC-3, CC-6, CC-7, CC-10, CC-25, CC-27, CC-36, C5K, C7K, C10K, C15K, and C16K), which are less cracked and seem to have inclusions [process (1) in fig. S1].

FIB microsampling

Seven calcite grains (CC-3, CC-6, CC-7, CC-10, CC-25, CC-27, and CC-36) were extracted from the polished sections together with surrounding matrix for SR-XCT analyses using FIBs (Thermo Fisher Scientific, Helios NanoLab 3G CX, and Quanta 200 3DS, at Kyoto University) [process (2) in fig. S1]. Specific areas (~30 μm by 30 μm) were cut out to a depth of ~30 μm using a Ga^+ ion beam at 30 kV [e.g., an area bounded by a red box in fig. S1 (1)]. Subsequently, the blocks were lifted from the polished section and mounted on W-needles. The mounted samples were observed by SR-XCT in 3D [process (3) in fig. S1].

After the SR-XCT observation, two samples (CC-6 and CC-7) were sliced into some pieces of regions of interest (ROIs) that have many nanosized inclusions for FE-TEM using the FIB [process (4) in fig. S1]. Slices for FE-S/TEM were also extracted from the five different calcite grains (CK5, CK7, CK10, CK15, and CK16) without

Downloaded from http://advances.sciencemag.org/ on May 6, 2021

京都大学 KYOTO UNIVERSITY
A Self-archived copy in
Kyoto University Research Information Repository
https://repository.kulib.kyoto-u.ac.jp
京都大学学術情報リポジトリ KURENAI 紅 Kyoto University Research Information Repository

performing SR-XCT. The sliced pieces were mounted on TEM grids and thinned to a thickness of ~300 nm using a Ga^+ ion beam at 30 kV. The thickness is thicker than conventional TEM sections (~100 nm or thinner) to prevent inclusion decrepitation (keep fluid in inclusions as far as possible, if present). The damaged layers formed on the ultrathin sections were removed using a Ga^+ ion beam at 2 kV.

We assessed the effect of heat damage by the FIB sample preparation. The temperature rise was calculated by using (*26*) with the average thermal conductivity of calcite (~4 W m^{-1} K^{-1}). We obtained ~<90- and ~27-K rise at the sample surface during sample thinning at <0.77 nA and final thinning at 0.083 nA, respectively. As the temperature rise in the central portion of the TEM sample is much smaller than that at the surface, we can rule out the possibility of the heat damage to the fluid.

SR-XCT experiment

The SR-XCT imaging experiment was performed for the seven samples at BL47XU of SPring-8, a synchrotron facility in Hyogo, Japan. SR-XCT enables us to obtain nondestructive 3D structure with high signal to noise ratios and high spatial resolution. We used two different methods: DET and SIXM. Details are described in (*3*).

Dual-energy tomography

The DET method is a tomography using x-ray absorption contrast for imaging (*7*), which gives us a spatial distribution of x-ray linear attenuation coefficients (LACs) of materials as a digital image. The LAC value, which is a function of the density, the elemental compositions of an object, and x-ray energy enable us to identify some mineral phases and their rough chemical compositions. The DET method was originally developed for iron-bearing samples to discriminate mineral phases with two different energies below and above the K-adsorption edge energy of iron (7.11 keV). Here, we used 7 and 8 keV. An imaging optical system with a Fresnel zone plate (FZP) was used to accomplish the submicrometer spatial resolution with the voxel size of 60 to 70 nm, which gives the effective resolution of ~200 nm. In the experiment, multiple projection images (1800 projections) were taken by rotating the sample in small intervals through a total of 180° (0.1° per projection). 3D CT images were reconstructed from the projection images using a convolution back-projection algorithm.

We easily recognized calcite and Fe-bearing minerals (serpentine, tochilinite, and cronstedtite) in the matrix. Inclusions in calcite and pores in the matrix were also easily recognized by their LAC values of almost zero at both 7 and 8 keV. Even if the inclusions are small, we can recognize these by edge-enhanced contrast, which is seen as a pair of bright and dark lines along mineral inclusion boundaries because of the refraction of x-rays. However, we cannot discriminate low-LAC materials such as water and organics from pore (air) by the absorption contrasts alone.

Scanning imaging x-ray microscopy

SIXM is a hybrid tomography system consisting of scanning x-ray microscope optics with 1D focusing (line-focusing) device and imaging x-ray microscope optics with a 1D objective (*8*). In the experiment, samples were illuminated with a line-focused beam and the transmitted and deflected x-ray beams were recorded in a 2D image detector. By rotating and scanning the samples with the line-focused beam, we can obtain both CT images of x-ray differential phase contrasts and x-ray absorption contrasts at the same time. We only used the phase-contrast images because absorption contrast images with higher resolution and less noise than SIXM were obtained by DET.

The phase-contrast images are a spatial distribution of x-ray RID, δ, of an object, which is the difference of x-ray refractive index, *n*, from unity

$$n = 1 - \delta \quad (1)$$

The RID value is a function of x-ray energy almost irrespective of the element species and is closely proportional to the density of the object. Furthermore, the phase contrast has a higher sensitivity than the absorption contrast in particular for light elements, where the RID/LAC sensitivity ratio exceeds a thousand. Therefore, the RID values are useful for discriminating materials particularly formed by light elements such as water and organics from air (Fig. 1D), which cannot be discriminated by the LAC values in x-ray absorption images. Here, the SIXM experiment was performed at 8 keV. Multiple projection images (750 projections) were taken by rotating the sample in small intervals through a total of 180° (0.24° per projection). Horizontal scan pitch was set to ~100 nm. Both phase and absorption CT images in 3D were reconstructed by a convolution back-projection algorithm. The voxel size of the CT images is ~100 nm, which results in an effective spatial resolution of about a few hundreds of nanometers.

In the phase-contrast images, nanosized inclusions are more poorly recognized than in the absorption images because the edge-enhanced contrast seen in DET images is not produced in the SIXM (Fig. 1, B and C). Nevertheless, we can determine whether water (or organics) is present inside micrometer-sized inclusions by using the RID values (Fig. 1D). If an inclusion is small, the RID values become larger than the real RID values because of overlapping of the two point spread functions from the both calcite walls as shown in a micrometer-sized inclusion (m-inc) in the A-A′ section of Fig. 1D. However, a RID value smaller than the RID value of water and liquid CO_2 shows that the inclusion is fluid free.

Image processing and analysis

As the LAC and RID values obtained by the reconstruction are slightly smaller than the real values, we corrected the LAC and RID values by calibration using standard materials as performed in (*3*). We searched for inclusions in the CT images by both DET and SIXM, and their locations in the samples in 3D were recognized using an open source image processing package "Fiji-ImageJ." Inclusions in calcite grains were digitally extracted by binarization of 3D-CT images, and their bird's-eye views were made (Fig. 1, E to G) using the software Slice (*27*).

FE-S/TEM experiments

FE-S/TEM-EDS observation and elemental analysis at room temperature

The ultrathin sections made from the two XCT samples and directly from the five grains were analyzed using a FE-S/TEM (JEOL, JEM-2100F, at Kyoto University) with an EDS (JEOL, JED-2300T) operated at 200 kV [process (5) in fig. S1]. TEM images were recorded using charge-coupled device cameras (Gatan, Orius 200D and Orius 1000A) and analyzed using the software package Gatan Digital Micrograph. Crystal structural identification was based on SAED patterns (Fig. 3 and fig. S2). The SAED patterns were analyzed using the software package ReciPro (*28*). The crystallographic

Downloaded from http://advances.sciencemag.org/ on May 6, 2021

京都大学 KYOTO UNIVERSITY
A Self-archived copy in
Kyoto University Research Information Repository
https://repository.kulib.kyoto-u.ac.jp
京都大学学術情報リポジトリ KURENAI 紅 Kyoto University Research Information Repository

orientation of the facets was estimated from the TEM image and SAED (fig. S2). We also acquired annular dark-field STEM (ADF-STEM) images and x-ray spectra and their elemental maps using the STEM-EDS system (figs. S3 and S4). Elemental maps containing data of x-ray intensities in individual pixels were acquired by scanning a focused electron beam with beam current (10 to 100 pA) at a high speed (0.1 ms per point) to avoid the x-ray count decrement caused by electron beam irradiation damage. No quantitative analysis was made. The identities of trapped or daughter crystals in some inclusions, such as Na-Mn and Fe sulfates, FeOOH (or Fe_2O_3) (fig. S3), and apatite (Fig. 2C and fig. S5), were estimated by their EDS elemental maps and spectrum, but are too small to be defined by SAED.

FE-S/TEM-EDS observation using a cryo-stage

After the TEM observation and analysis at room temperature, we transferred the TEM samples from a conventional stage to a cryo-stage (Gatan, 636 double tilt liquid nitrogen cooling holder) and observed fluid inclusion candidates, which are relatively large and may preserve fluid based on the room temperature observation (<100 nm in size, apart from twin boundaries, and having a relatively dark contrast in TEM bright field), at 173 and 293 K using the same FE-TEM with the same observation conditions except for the temperature. It took about less than 30 and 90 min to decrease and increase the temperature between 293 and 173 K, respectively, but we waited for about ~60 and 180 min, respectively, to stabilize the temperatures and the stage drift before measurements were made.

We obtained SAED patterns of the fluid inclusion candidates at 293 and 173 K to detect any extra spots by frozen product(s) of possible fluid at 173 K (Fig. 3). Only one inclusion showed a definitely clear SAED pattern of extra spots of ice. This may suggest that the probability of the presence of fluid is originally very small. Another possibility is the loss of fluids (decrepitation) from many inclusions during the long history of the meteorite, preparation of the samples by FIB microsampling, handling of the TEM samples by mechanical disturbance including thermal stress, and/or observation under SEM and TEM by electron beam irradiation.

SUPPLEMENTARY MATERIALS

Supplementary material for this article is available at http://advances.sciencemag.org/cgi/content/full/7/17/eabg9707/DC1

REFERENCES AND NOTES

1. W. Fujiya, P. Hoppe, T. Ushikubo, K. Fukuda, P. Lindgren, M. R. Lee, M. Koike, K. Shirai, Y. Sano, Migration of D-type asteroids from the outer Solar System inferred from carbonate in meteorites. *Nat. Astron.* **3**, 910–915 (2019).
2. M. Yoshikawa, J. Kawaguchi, A. Fujiwara, A. Tsuchiyama, Hayabusa sample return mission, in *Asteroids IV* (University of Arizona, 2015), pp. 397–418.
3. M. Matsumoto, A. Tsuchiyama, A. Nakato, J. Matsuno, A. Miyake, A. Kataoka, M. Ito, N. Tomioka, Y. Kodama, K. Uesugi, A. Takeuchi, T. Nakano, E. Vaccaro, Discovery of fossil asteroidal ice in primitive meteorite Acfer 094. *Sci. Adv.* **5**, eaax5078 (2019).
4. M. E. Zolensky, R. J. Bodnar, H. Yurimoto, S. Itoh, M. Fries, A. Steele, Q. H.-S. Chan, A. Tsuchiyama, Y. Kebukawa, M. Ito, The search for and analysis of direct samples of early Solar System aqueous fluids. *Phil. Trans. R. Soc. A* **375**, 20150386 (2017).
5. M. E. Zolensky, R. J. Bodnar, E. K. Gibson Jr., L. E. Nyquist, Y. Reese, C.-Y. Shih, H. Wiesmann, Asteroidal water within fluid inclusion-bearing halite in an H5 chondrite, Monahans (1998). *Science* **285**, 1377–1379 (1999).
6. Y. Kebukawa, M. Ito, M. Zolensky, Z. Rahman, H. Suga, A. Nakato, Q. H. S. Chan, M. Fries, Y. Takeichi, Y. Takahashi, K. Mase, K. Kobayashi, A novel organic-rich meteoritic clast from the outer solar system. *Nat. Sci. Rep.* **9**, 3169 (2019).
7. A. Tsuchiyama, T. Nakano, K. Uesugi, M. Uesugi, A. Takeuchi, Y. Suzuki, R. Noguchi, T. Matsumoto, J. Matsuno, T. Nagano, Y. Imai, T. Nakamura, T. Ogami, T. Noguchi, M. Abe, T. Yada, A. Fujimura, Analytical dual-energy microtomography: A new method for obtaining three-dimensional mineral phase images and its application to Hayabusa samples. *Geochim. Cosmochim. Acta* **116**, 5–16 (2013).
8. A. Takeuchi, K. Uesugi, Y. Suzuki, Three-dimensional phase-contrast X-ray microtomography with scanning-imaging X-ray microscope optics. *J. Synchrotron Rad.* **20**, 793–800 (2013).
9. J. Longhi, Phase equilibria in the system CO2-H2O I: New equilibrium relations at low temperatures. *Geochim. Cosmochim. Acta* **69**, 529–539 (2005).
10. G. J. Vogt, K. S. Pitzer, Entropy and heat capacity of methane; spin-species conversion. *J. Chem. Thermodynam.* **8**, 1011–1031 (1976).
11. D. R. Lide, *CRC Handbook of Chemistry and Physics, 88th Edition 2007–2008* (CRC Press, Taylor & Francis, 2007), pp. 3–88.
12. D. Kralj, L. Brečević, Dissolution kinetics and solubility of calcium carbonate monohydrate, colloids and surfaces. *Colloids Surf. A Physicochem. Eng. Asp.* **96**, 287–293 (1995).
13. M. Bruno, F. R. Massaro, L. Pastero, E. Costa, M. Rubbo, M. Prencipe, D. Aquilano, New estimates of the free energy of calcite/water interfaces for evaluating the equilibrium shape and nucleation mechanisms. *Cryst. Growth Des.* **13**, 1170–1179 (2013).
14. M. J. Mumma, S. B. Charnley, The chemical composition of comets - emerging taxonomies and natal heritage. *Annu. Rev. Astron. Astrophys.* **49**, 471–524 (2011).
15. R. J. Bakker, J. B. H. Jansen, A mechanism for preferential H_2O leakage from fluid inclusions in quartz, based on TEM observations. *Contrib. Mineral. Petrol.* **116**, 7–20 (1994).
16. A. J. Brearley, The action of water, in *Meteorites and the Early Solar System II* (The University of Arizona Space Science Series, 2006), pp. 587–622.
17. S. Okuzumi, M. Momose, S.-i. Shirono, H. Kobayashi, H. Tanaka, Sintering-induced dust ring formation in protoplanetary disks: Application to the HL tau disk. *Astron. J.* **821**, 82 (2016).
18. K. J. Walsh, A. Morbidelli, S. N. Raymond, D. P. Óbrien, A. M. Mandell, Populating the asteroid belt from two parent source regions due to the migration of giant planets—"The Grand Tack". *Meteorit. Planet. Sci.* **47**, 1941–1947 (2012).
19. H. F. Levison, W. F. Bottke, M. Gounelle, A. Morbidelli, D. Nesvorný, K. Tsiganis, Contamination of the asteroid belt by primordial trans-Neptunian objects. *Nature* **460**, 364–366 (2009).
20. P. H. Warren, Stable-isotopic anomalies and the accretionary assemblage of the Earth and Mars: A subordinate role for carbonaceous chondrites. *Earth Planet. Sci. Lett.* **311**, 93–100 (2011).
21. T. S. Kruijer, C. Burkhardt, G. Budde, T. Kleine, Age of Jupiter inferred from the distinct genetics and formation times of meteorites. *Proc. Natl. Acad. Sci. U.S.A.* **114**, 6712–6716 (2017).
22. S. J. Desch, A. Kalyaan, C. M. O'D. Alexander, The effect of Jupiter's formation on the distribution of refractory elements and inclusions in meteorites. *Astrophys. J. Suppl. Ser.* **238**, 11–41 (2018).
23. M. Zolensky, T. Mikouchi, M. Fries, R. Bodnar, P. Jenniskens, Q.-z. Yin, K. Hagiya, K. Ohsumi, M. Komatsu, M. Colbert, R. Hanna, J. Maisano, R. Ketcham, Y. Kebukawa, T. Nakamura, M. Matsuoka, S. Sasaki, A. Tsuchiyama, M. Gounelle, L. Le, J. Martinez, K. Ross, Z. Rahman, Mineralogy and petrography of C asteroid regolith: The Sutter's Mill CM meteorite. *Meteorit. Planet. Sci.* **49**, 1997–2016 (2014).
24. A. Miyake, J. Matsuno, S. Toh, Sample preparation toward seamless 3D imaging technique from micrometer to nanometer scale. *Microscopy* **63**, i24–i25 (2014).
25. M. R. Lee, P. Lindgren, M. R. Sofe, Aragonite, breunnerite, calcite and dolomite in the CM carbonaceous chondrites: High fidelity recorders of progressive parent body aqueous alteration. *Geochim. Cosmochim. Acta* **144**, 126–156 (2014).
26. T. Ishitani, H. Kaga, Calcultion of local temperature rise in focused-ion-beam sample preparation. *J. Electron Microsc.* **44**, 331–336 (1995).
27. T. Nakano, A. Tsuchiyama, K. Uesugi, M. Uesugi, K. Shinohara, *"Slice"—Softwares for Basic 3-D Analysis* (Japan Synchrotron Radiation Research Institute, 2006).
28. Y. Seto, D. Nishio-Hamane, T. Nagai, N. Sata, Development of a software suite on X-ray diffraction experiments. *Rev. High Press. Sci. Tech.* **20**, 269–276 (2010).
29. L. N. Plummer, E. Busenberg, The solubilities of calcite, aragonite and vaterite in CO_2–H_2O solutions between 0° and 90°C, and an evaluation of aqueous model for the system $CaCO_3$–CO_2–H_2O. *Geochim. Cosmochim. Acta* **46**, 1011–1040 (1982).
30. G. J. Consolmagno, D. T. Britt, R. J. Macke, The significance of meteorite density and porosity. *Chemie der Erde* **68**, 1–29 (2008).
31. J. W. Morse, F. T. Maclenzie, *Geochemistry of Sedimentary Carbonates* (Elsevier Scientific Pub. Co. Inc., 1990), 707 pp.
32. D. Lynden-Bell, J. E. Pringle, The evolution of viscous discs and the origin of the nebular variables. *Mon. Not. R. Astron. Soc.* **168**, 603–637 (1974).
33. E. I. Chiang, P. Goldreich, Spectral energy distributions of T Tauri stars with passive circumstellar disks. *Astrophys. J.* **490**, 368–376 (1997).
34. N. I. Shakura, R. A. Sunyaev, Black holes in binary systems. Observational appearance. *Astron. Astrophys.* **24**, 337–355 (1973).
35. K. R. Bell, D. N. C. Lin, Using FU Orionis outbursts to constrain self-regulated protostellar disk models. *Astrophys. J.* **427**, 987–1004 (1994).

Downloaded from http://advances.sciencemag.org/ on May 6, 2021

京都大学 KYOTO UNIVERSITY
A Self-archived copy in
Kyoto University Research Information Repository
https://repository.kulib.kyoto-u.ac.jp
京都大学学術情報リポジトリ KURENAI 紅 Kyoto University Research Information Repository

Acknowledgments: The SR-XCT experiments at SPring-8 in this study were conducted under proposal numbers 2013A1462, 2013B1459, 2014A1453, 2015A1358, 2015A1413, 2015B1309, and 2016A1253. **Funding:** A.Ts. and K.U. were supported by JSPS KAKENHI grant number JP15H05695. A.Ts. was also supported by grant number JP20H00205 and by Chinese Academy of Sciences President's International Fellowship Initiative grant number 2019VCA0004. A.M. and K.U. were supported by JSPS KAKENHI grant number JP16H06348. S.O. was supported by JSPS KAKENHI grant numbers JP18H05438 and JP19K03926. M.Z. was supported by the NASA Emerging Worlds Program. **Author contributions:** A.Ts. and A.K. contributed to this paper mainly by SEM and SR-XCT works; A.M. by SR-XCT, TEM, and FIB works; K.U., A.Ta., and T.N. by SR-XCT works; S.O. by discussion about theoretical planetesimal formation model; and J.K. by discussion about carbonate dissolution and precipitation. All of the authors contributed to discussion. All authors contributed equally. **Competing interests:** The authors declare that they have no competing interests. **Data and materials availability:** All data needed to evaluate the conclusions in the paper are present in the paper and/or the Supplementary Materials. Additional data related to this paper may be requested from the authors. The software Slice (developed by T. Nakano *et al.*) and Fiji-ImageJ used for the x-ray CT image analysis are available in the websites http://www-bl20.spring8.or.jp/slice and https://imagej.net/Fiji, respectively. The software ReciPro used for TEM data analyses (developed by Y. Seto) is available in the website http://pmsl.planet.sci.kobe-u.ac.jp/~seto/. The database for calculation of the RID values is available in the website http://henke.lbl.gov/optical_constants/.

Submitted 7 February 2021
Accepted 5 March 2021
Published 21 April 2021
10.1126/sciadv.abg9707

Citation: A. Tsuchiyama, A. Miyake, S. Okuzumi, A. Kitayama, J. Kawano, K. Uesugi, A. Takeuchi, T. Nakano, M. Zolensky, Discovery of primitive CO_2-bearing fluid in an aqueously altered carbonaceous chondrite. *Sci. Adv.* **7**, eabg9707 (2021).

Downloaded from http://advances.sciencemag.org/ on May 6, 2021

京都大学 KYOTO UNIVERSITY
A Self-archived copy in
Kyoto University Research Information Repository
https://repository.kulib.kyoto-u.ac.jp
京都大学学術情報リポジトリ KURENAI 紅 Kyoto University Research Information Repository

Science Advances

Discovery of primitive CO_2-bearing fluid in an aqueously altered carbonaceous chondrite

Akira Tsuchiyama, Akira Miyake, Satoshi Okuzumi, Akira Kitayama, Jun Kawano, Kentaro Uesugi, Akihisa Takeuchi, Tsukasa Nakano and Michael Zolensky

Sci Adv **7** (17), eabg9707.
DOI: 10.1126/sciadv.abg9707

ARTICLE TOOLS http://advances.sciencemag.org/content/7/17/eabg9707

SUPPLEMENTARY MATERIALS http://advances.sciencemag.org/content/suppl/2021/04/19/7.17.eabg9707.DC1

REFERENCES This article cites 30 articles, 3 of which you can access for free
http://advances.sciencemag.org/content/7/17/eabg9707#BIBL

PERMISSIONS http://www.sciencemag.org/help/reprints-and-permissions

Use of this article is subject to the Terms of Service

Science Advances (ISSN 2375-2548) is published by the American Association for the Advancement of Science, 1200 New York Avenue NW, Washington, DC 20005. The title *Science Advances* is a registered trademark of AAAS.

Copyright © 2021 The Authors, some rights reserved; exclusive licensee American Association for the Advancement of Science. No claim to original U.S. Government Works. Distributed under a Creative Commons Attribution NonCommercial License 4.0 (CC BY-NC).

Downloaded from http://advances.sciencemag.org/ on May 6, 2021